RSC Advances

ROYAL SOCIETY OF CHEMISTRY

www.rsc.org/advances

Journal Name

ARTICLE

One-pot synthesis of triazine-framework derived catalysts with high performance for polymer electrolyte membrane fuel cells

Received 00th January 20xx,
Accepted 00th January 20xx

DOI: 10.1039/x0xx00000x

www.rsc.org/

Yong You[a,b], Chenghao Wu[a,b], Yingfang Yao[a,b], Jianguo Liu[a,b,c]*, Zhongwei Wang[a,b], Lin Huang[a,b], Jin Xie[a,b], Xiaogang Su[a,b] and Zhigang Zou[a,b,c]**

The prohibitive cost and scarcity of the precious metals used for oxygen reduction reaction (ORR) catalysts limit the large-scale commercialization of proton exchange membrane fuel cell (PEMFC). Great efforts have been made to improve the ORR activity of non-precious metal catalyst. Herein, we describe a one-pot synthetic process of preparing triazine-polymer-Fe-C catalyst using polyimide (PI), ferric chloride and melamine as the precursors with a pronounced electrocatalytic activity towards ORR in acid media. The ORR activity of catalysts and the performance of single cells strongly depend on the properties of the carbon supports, which affect the surface areas and microporosities of the final catalysts. The optimized PI-Fe-C catalyst exhibits an excellent performance (onset potential of 0.92V and the half-wave potential 0.78V) towards ORR activity in acid medium. A maximum power density of 310 $mW \cdot cm^{-2}$ is obtained with a loading of 2 $mg \cdot cm^{-2}$ in a single cell.

1. Introduction

Proton exchange membrane fuel cells (PEMFCs) are widely recognized as one of the most promising energy conversion technologies to replace internal combustion engines for automotive propulsion, due to the high energy yield, low environmental impact and simple design [1-3]. The large scale application of PEMFCs requires highly active and durable catalysts for oxygen reduction reaction (ORR) [4-6]. Currently, the state-of-the-art catalysts for fuel cell use are based on precious metals [7, 8], for example, platinum. However, disadvantages, such as the scarcity, prohibitive cost and limited durability of these noble metals hamper the large-scale commercialization of PEMFCs. Accordingly, extensive efforts have been directed to the development of low-cost non-precious metal catalysts (NPMCs) with high performance to reduce the cost of PEMFCs. Among various NPMCs, the catalysts synthesized from heat treatment of carbon, nitrogen–containing compounds with M (M = Fe, Co) salt precursors exhibit excellent performance on ORR, considered as a promising substitute for Pt or Pt alloys [9, 10].

It is well recognized that in electrochemical systems, the processes and factors that affect the transport of charge across the interface between chemical phases are generally concerned, including electrochemical catalysis [11]. As a result, electrocatalysts with porous structure, especially highly connected nano-scale pores facilitating gas diffusion, and large surface area generally refer to better performance, especially for those reactions with gas phase mass, such as air-breathe cathode for metal-air batteries [12, 13], NH_3, gas sensors [14-16], and so forth. And this fact is similar to those catalysts for PEMFCs [17]. It has been verified that the electrochemical surface areas for ORR, i.e. catalytically active sites, highly influences the fuel cell performance during operation processes [18-22]. For example, higher electrochemical surface areas of Pt-based catalysts generally result in more prominent electrocatalytic activities and ORR performance [18, 23]. As a result, NPMCs for ORR with porous structure leading to better catalytical performance is high anticipated.

Recently, Fe-N-C catalysts were mainly fabricated from the nitrogen contained polymers with dense structure, for example, polyaniline (PANI), or polypyrrole (PPY) [3]. Because of the straight-chain structure of this type of polymer, it was possible for iron precursors to be buried in the dense skeleton of polymer matrix during the polymerization. After pyrolysis, a quite questionable issue could not be ignored that a proportion of catalytic sites might be embedded in the bulk of the carbon matrix, which could hardly make contributions to the reduction of O_2 due to the isolation of active sites with oxygen molecules. Only the part of active sites exposed to the solid-gas interfaces would catalyze ORR. As a result, the potential performance could not be exhibited ultimately. Employing porous polymer as precursors may effectively avoid this problem. After pyrolysis, more three-phase boundaries formed and active sites could mainly deploy on these three-phase boundaries, thus enhancing ORR activity. Therefore, it is quite meaningful to

[a] Department of Materials Science and Engineering, National Laboratory of Solid State Microstructures, Collaborative Innovation Center of Advanced Microstructures, Nanjing University, 22 Hankou Road, Nanjing 210093, China.
[b] Eco-materials and Renewable Energy Research Center, Jiangsu Key Laboratory for Nano Technology, Nanjing University, 22 Hankou Road, Nanjing 210093, China.
[c] Kunshan Sunlaite New Energy Co. ltd, Kunshan Innovation Institute of Nanjing University, Jiangsu, China 215347
* Corresponding author. Tel.:+86 25 83621219; Fax: +86 25 83686632, E-mail address: jianguoliu@nju.edu.cn.
** Corresponding author. Tel.:+86 25 83686630; Fax: +86 25 83686632, E-mail address: zgzou@nju.edu.cn

exploring porous materials with low density to prepare high performance catalysts.

Triazine-based framework polymers might be a good candidate as the precursor to fabricate highly porous NPMCs. Used in the areas of photocatalysis, hydrogen storage, gas adsorption and separation, triazine-based framework polymers were famous as 2D or 3D porous solids for their intrinsic microporosity and high surface area [24-28]. Owing to their superior porosity properties, it is rational to use this type of polymer as the precursor of NPMCs. And such a nitrogen-containing polymer leads to a uniform distribution of nitrogen sites on the catalysts surface and an increase in the surface density of catalytic sites that conduce to the improvement in ORR activity. Thus, the triazine-based framework polymers were considered as a potential material to fabricate catalysts with pronounced ORR activity. Herein we fabricated a triazine-based polyimide (PI) as the precursor of NPMCs. During the fabrication procedure, Fe^{3+} was induced. After pyrolysis, a series of carbon-supported NPMCs with large surface area and ORR activities were obtained. For the purpose of the verification of the effect of surface area to the ORR activities, different carbon support materials were employed for comparison. The triazine-framework derived NPMCs were fabricated with a facile, low cost, one-pot synthetic process, which demonstrated that this type of ORR catalysts have the potential for large commercialization.

2. Experimental Section

2.1 Reagents

Vulcan XC-72 and Black pearls (BP) 2000 were purchased from CARBOT (America). Ketjenblack (KJ) EC-300J was obtained from LION Corporation (Japan). Melamine(MA) (99wt%) and pyromellitic Dianhydride (PMDA) (99wt%) were purchased from Aladdin Industrial Corporation (America). Ferric chloride hexahydrate ($FeCl_3 \cdot 6H_2O$) (analytical grade) was purchased from Shanghai Chemical Reagent Co. (China).

2.2 Preparation of PI-Fe-C catalyst

Ferric chloride hexahydrate($FeCl_3$), MA(Melamine), PMDA (pyromellitic Dianhydride) and carbon support were simply placed in the ball milling vial to undergo 60 minutes of ball milling. The homogeneous mixture was put into porcelain crucible and heated at 10 ℃ min^{-1} up to 325 ℃ for 4 h to allow the polymerization between MA and PMDA to form the PI in the tube furnace under an inert atmosphere of nitrogen gas. And then the intermediate product was pyrolyzed 900 ℃ for 1 h to obtain the final catalyst. The catalysts prepared with the (Black pearls (BP) 2000, Ketjenblack (KJ) EC-300J, Vulcan XC-72) were denoted as PI-Fe-BP, PI-Fe-EC and PI-Fe-XC.

2.3 Physical characterizations

Transmission electron microscopy (TEM) images were obtained with a field-emission transmission electron microscope (Tecnai G2 FEI). The specific surface area was collected through Brumauer–Emmett–Teller (BET) method by N_2 adsorption (TriStar-3000, Micromeritics, USA). The crystal structures of the catalyst sample was characterized by a powder X-ray diffractometer (XRD, Ultima III, Rigaku Corp., Japan) using Cu-Kα radiation (λ = 1.54178 Å, 40 kV, 40 mA). The surface composition of the samples was characterized by using X-ray photoelectron spectroscopy (XPS, ESCALAB 250).

2.4 Electrochemical characterization

The catalysts' performance for ORR was measured using the rotating disk electrode (RDE) technique in 0.1M $HClO_4$ aqueous solution. All measurements was conducted in a thermostat-controlled, standard three-electrode cell at room temperature, in which the platinum foil ,a reversible hydrogen electrode (RHE) and a rotating glassy carbon (GC) disk electrode were used as the counter electrode, the reference electrode and the working electrode, respectively. The catalyst "ink" was prepared by ultrasonically mixing for one hour a mass of 10 mg of catalyst with 95μL of a 5wt% Nafion solution (Aldrich) and 350μL of ethanol. And then an aliquot of 7μL was pipetted onto a glassy carbon disk surface (0.19625 cm^2), resulting in a catalyst loading (iron plus carbon black) of 800μg·cm^{-2}. The solution was dried in air at room temperature. Meanwhile, 0.1 M $HClO_4$ aqueous solution **s**aturated with oxygen by bubbling O_2 for 30 min served as the supporting electrolyte. Steady cyclic voltammetry was performed in a potential range of 0 to 1.2 V vs. reversible hydrogen electrode (RHE) at a scan rate of 50 mV·s^{-1}. During cyclic voltammetry process, a flow of O_2 was maintained over the electrolyte solution for continued O_2 saturation. For the ORR measurements using RDE technique, the PI-Fe-C modified GC electrode was rotated at speeds 900 rpm in O_2 saturated 0.1 M $HClO_4$ aqueous solution, and the RDE current voltage curves were measured at a potential scan rate of 10 mV·s^{-1}. For measurements using Rotating Ring Disk Electrode (RRDE), which were used to detect the H_2O_2 produced during the ORR process, the same conditions as in the RDE experiments were used, with an electrode containing a Pt ring (6.25 mm inner diameter and 7.92 mm outer diameter) and a GC disk (5.61 mm diameter) employed as the working electrode. The catalyst ink was prepared in the same way as for the RDEs. An amount of ink was loaded on the GC rotating disk electrode to keep the same catalyst loading as in the RDE measurements. A potential of 1.20 V vs. reversible hydrogen electrode (RHE) was applied to the Pt ring electrode, which had a collection efficiency of 0.37.

2.5 Single cell testing

A MEA (Membrane Electrode Assembly) was fabricated by decal transfer method. The cathode catalyst powder was dispersed in a mixture of Nafion solution (5wt%, Aldrich), ethanol and deionized water. The dry catalyst/Nafion ratio was 1/1.5. The obtained catalyst "ink" was then applied to the gas diffusion layer (GDL, Sunrise Power Inc. China) until the cathode catalyst loading reached 2mg·cm^{-2}.The anode catalyst was 60wt% Pt/C from Johnson Matthey with a loading of 0.4 mg Pt cm^{-2}, and the Nafion content in anodic catalyst layer was 33wt%. Then, the MEA was prepared by hot-pressing the electrodes and Nafion 211 membrane with an active area of 2.0 cm^{-2}.

Fuel cell polarization curve was tested at 80 ℃ on a fuel cell test system (Model 850e, Scribner Associates Inc.). H_2 and O_2 flow rates were 300 ml·min^{-1} at 100% RH, and no back pressure was applied (i.e., the O_2 and H_2 partial pressure was about 0.53 bar since the saturation water vapor pressure at 80 ℃ is ca 0.47 bar). The polarization curve was recorded by scanning the cell voltage from open circuit potential down to 0.1 V at a scan rate of 0.5 mV·s^{-1}.

3. Result and Discussion

The schemetic synthetic process of triazine framework derived electrocatalysts was shown in Fig. 1. In a typical process, the catalyst preparation simply involved the synthesis of Fe contained polyimide (PI) as the precursor, followed by pyrolysis to yield the final PI-Fe-C catalysts. Compared with the catalysts prepared from the other 'two-step' methods[29], that the PI-Fe-C catalysts with pronounced ORR activity were obtain from the facile synthesis process suggested that this type of ORR catalysts have the potential for large commercialization.

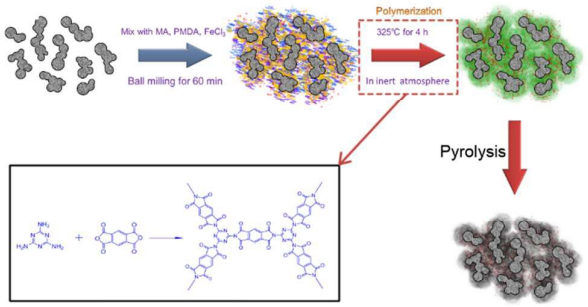

Fig.1 The schemetic synthesis procedure of PI-Fe-C catalysts.

The structure and morphology of the typical catalyst, PI-Fe-BP, was investigated by TEM. As shown in Fig. 2a, b, c, the nanoparticles with an average diameter of ~50 nm were coated with a carbonized layers with the thickness of several nanometers. The phase composition and structure of the samples prepared with different carbon support materials were examined by XRD shown in Fig. 2d. For all samples, the broad peak at about 26.5° was assigned to the [002] planes of the hexagonal graphite structure[28], indicating the presence of highly graphitic carbon. And the diffraction peaks at around 45° were characteristic reflections of crystalline Fe_3C in the materials which were synthesized with $FeCl_3$ [30-32]. Even though the crystallization of Fe_3C is slightly enhanced with the decrease of surface areas of the carbon materials, the XRD pattern confirms the presence of graphitic carbon and Fe_3C phases, which demonstrated the similarity
of phase composition and structure of the samples. It has been reported the little contribution of metallic Fe particles to ORR activity[33]. And no observation of metallic Fe in catalysts indicated the successful synthesis of ORR catalytic materials.

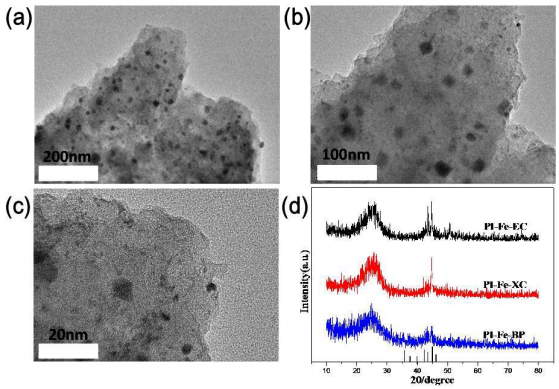

Fig. 2(a, b, c) TEM images of the catalyst PI-Fe-BP at different magnifications.The catalyst obtained from pyrolysis at 900 ℃ with BP2000 as the template, nominated as PI-Fe-BP. (d) XRD patterns of the catalysts prepared with various carbon materials.

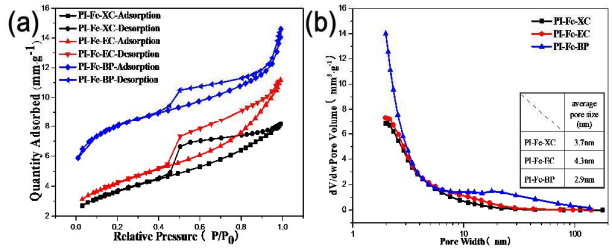

Fig.3 (a) Nitrogen adsorption–desorption isotherms of PI–Fe–C catalysts with different carbon support materials. (b) The BJH pore size distribution of catalysts with different carbon support materials. Inset shows the average pore sizes.

The Brunauer–Emmett–Teller (BET) specific surface areas of these three catalysts were determined by the low-temperature nitrogen absorption method. Fig. 3a shown the nitrogen adsorption-desorption isotherms and pore size distribution of the PI-Fe-XC, PI-Fe-EC, PI-Fe-BP at 77k. A distinct hysteresis loop can be observed in the larger range of ca. 0.45–1.0 P/P_0, indicating the presence of a mesoporous structure. The average pore sizes of these three catalysts, as shown in Fig. 3b, calculated from desorption data using the BJH model were 2.9 nm, 3.7 nm, 4.3 nm. It is apparent that the high surface areas of the catalysts mainly result from the mesoporous structure. The catalyst PI-Fe-BP shown a highest BET surface area of 624 $m^2 \cdot g^{-1}$, while the BET surface areas of PI-Fe-XC and PI-Fe-EC were 290 $m^2 \cdot g^{-1}$ and 334 $m^2 \cdot g^{-1}$. The micropore area for PI-Fe-BP, PI-Fe-EC and PI-Fe-XC were292 $m^2 \cdot g^{-1}$, 163$m^2 \cdot g^{-1}$ and 50 $m^2 \cdot g^{-1}$, respectively. For these carbon supported catalysts**,** the carbon support of the catalysts can not only be deemed as materials constructing electrons generated in the ORR process but also an in situ template for carbon nanostructures with specific morphology during the preparation procedure of catalysts. Due to the highest area and porosity of BP2000 among these three carbon supports, the obtained PI-Fe-BP catalyst exhibited highest surface area and porosity. It also illuminated why the surface areas and porosity of PI-Fe-EC were larger than that of PI-Fe-XC (the surface areas of Ketjenblack (KJ) EC-300J is larger than Vulcan XC-72).

The ORR activity of PI-Fe-C catalysts was determined using RDE technique as shown in Fig. 4a. The PI-Fe-EC catalyst shared a similar

onset potential of 0.87 V with PI-Fe-XC catalyst. And the PI-Fe-BP catalyst show the most positive onset potential of 0.92 V. The limiting current density of the catalysts increased with the increase of surface area of carbon support used for the catalysts. And the kinetic current density (Fig. 4b) at 0.8 V increases from –0.49 $mA{\cdot}cm^{-2}$ for PI-Fe-XC, –0.61 $mA{\cdot}cm^{-2}$ for PI-Fe-EC, to –1.55 $mA{\cdot}cm^{-2}$ for PI-Fe-BP. The PI-Fe-BP catalyst exhibits the most excellent electrocatalytic activity.

The performance of the single cell with PI-Fe-C cathode catalysts is shown in Fig. 4c. The open circuit voltages were separately 0.82 V, 0.79 V and 0.7 V with O_2. And the maximum power output were 310 $mW{\cdot}cm^{-2}$,150 $mW{\cdot}cm^{-2}$,110 $mW{\cdot}cm^{-2}$, respectively. For these three catalysts, the PI-Fe-BP exhibited most excellent performance in real fuel cell. Notably, the specific power was as high as 155 $W{\cdot}g^{-1}$ for PI-Fe-BP without back pressure applied. Although some catalysts prepared with Fe present showed similar or even better ORR activity and single cell performance, no Fe-based catalyst with such impressive specific activity in the environment without back pressure has been reported previously[34].

Generally, the micropores determined the onset potential. The similar onset potentials of 0.87 V between PI-Fe-XC and PI-Fe-EC observed in Fig. 4a were due to the close surface areas and micropore area, which provided almost the same density of active sites. But the higher limiting current density of the PI-Fe-EC in comparison to the PI-Fe-XC arises from the numerous pores, which enhanced mass transfer.

The most excellent catalytic performance of the PI-Fe-BP was attributed to the highest specific surface area and the high electrolyte-accessible surface area which enhanced utilization of nitrogen active sites led to a higher electrochemical activity. The high surface and numerous pores ought to provide high surface

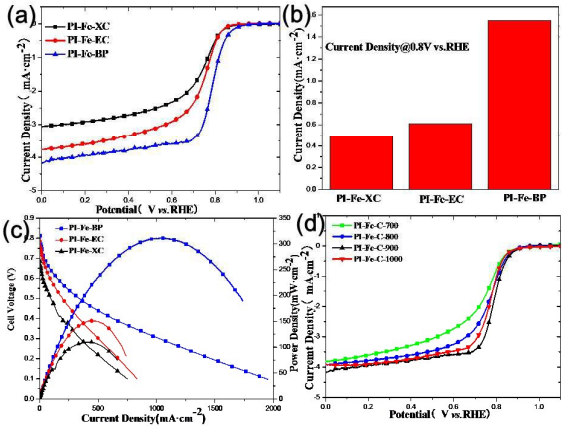

Fig.4 (a) ORR polarization curves of different carbon-supported PI–Fe–C catalysts recorded in an O_2-saturated 0.1 M $HClO_4$ aqueous solution at a sweep rate of 10 $mV{\cdot}s^{-1}$and a rotation rate of 900 rpm; (b) ORR performance of catalysts at 0.8 V vs. RHE. (c) Polarization and power density plots for H_2-O_2 single fuel cell with PI-Fe-C as cathode catalysts at 80 ℃. No back pressure was applied. (d) ORR polarization curves for catalysts obtained from different pyrolysis temperatures.

density of catalytic sites exposed to oxygen molecules and thus lead to the enhanced ORR activity. It also illustrated why the single cell with PI-Fe-BP catalyst shown remarkablely well performance. Compared with the other two catalysts, the high surface area and pore surface area of PI-Fe-BP would improve the catalyst`s ability of oxygen adsorption. The oxygen reduction reaction interface was enlarged and huge amounts of oxygen were reduced under the action of the catalysis of active sites in theses pores. Due to the poor ability of gas adsorption with respect to the PI-Fe-BP, the other two catalysts exhibited poor performance in single cells.

To elucidate the effect of the pyrolysis temperature, heat-treated $FeCl_3$ @polyimide (PI) supported by carbon black （Black pearls (BP) 2000）was prepared at various temperatures of 700, 800, 900 and 1000 ℃, which were denoted as PI-Fe-BP-700, PI-Fe-BP-800, PI-Fe-BP-900 and PI-Fe-BP-1000, respectively. Fig. 4d displayed the ORR curves for catalysts at various temperatures from 700 to 1000 ℃ in O_2 saturated 0.1 M $HClO_4$ solution. The ORR activity of the PI-Fe-BP catalysts had been found to increase with increasing the pyrolysis temperature from 700 to 900 ℃ and to decrease with increasing temperature from 900 to 1000 ℃. PI-Fe-BP-900 catalyst shows the highest ORR activity among these catalysts, based on both the onset potential and the limiting current density. Clearly, the pyrolysis temperatures played a critical role in enhancing the catalytic ORR activity.

Fig. 5a show the XRD pattern of the catalysts obtained at various

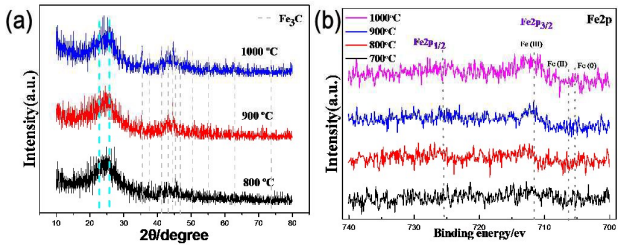

Fig. 5(a) XRD patterns of the catalysts prepared with various carbon materials. (b) The high resolution XPS spectra Fe 2p of catalysts obtained at different temperatures.

temperatures. The diffraction peaks were characteristic reflections of crystalline Fe_3C in the materials. The XPS spectra of these catalysts were obtained to analyze elemental quantification of the near-surface layers of samples treated at various temperatures. Table1 show the surface species concentration for various PI-Fe-BP catalysts prepared at different temperatures. The catalyst PI-Fe-BP-800

Table 1 Surface species concentration of PI-based catalysts with different heat-treatment temperatures.

Catalyst sample	Atomic concentration (at%)			
	C	O	N	Fe
PI-Fe-BP-700	95.71	2.24	1.98	0.07
PI-Fe-BP-800	95.31	3.19	1.41	0.09
PI-Fe-BP-900	96.85	2.27	0.79	0.09
PI-Fe-BP-1000	96.62	2.54	0.71	0.13

contained larger amounts of oxygen content than the catalyst PI-Fe-BP-700 and the oxygen content in PI-Fe-BP-1000 was higher than that of PI-Fe-BP-9000. The high pyrolysis temperature may increase the probability for oxygen incorporation as carbonyl groups [35]; hence, high pyrolysis temperature does not always lower oxygen

content. And previous studies have reported that the presence of a certain amount of oxygen is beneficial for the ORR.

With pyrolysis temperature rising from 700 to 1000 ℃, the near-surface iron content increased and the nitrogen content decreased monotonically. As can be seen from Fig. 5b, the Fe 2p spectrum was divided into Fe2p$_{3/2}$ and Fe2p$_{1/2}$ centered at 711.2 and 725.1 eV, respectively. The dash-lines indicated the average binding energies of Fe^0 (iron carbides (706.7–706.9 eV)), Fe^{2+} (707–708.7 eV), and Fe^{3+} (711.2–720.1 eV)[36].This suggests the existence of iron in different chemical states except the phase of Fe_3C.

The near-surface nitrogen content was generally considered to play a crucial role in ORR activity. However, the ORR activity of these catalysts does not change monotonically with temperature, suggesting no direct correlation between activity and the total amount of near-surface elemental content, especially incorporated nitrogen content as elsewhere claimed [37]. In the present reports, even the PI-Fe-C-900 catalyst which contained second lowest total nitrogen content (about 0.79 at%) was more active than the other two catalysts with higher total nitrogen content, obtained at the temperature of 700 ℃, 800 ℃, respectively. The phenomenon indicated that the content of nitrogen doped in these materials was sufficient and should not limit the ORR activity.

The N 1s XPS spectra for these catalysts were shown in Fig. 6. All samples were fitted to three N-containing functional groups based on the bonding state of the N atom, which included pyridinic N (~398.6 eV), quaternary N (~400.7 eV) and C-N^+ (~401.5 eV). The content and relative atomic ratios of different types of nitrogen changed with the pyrolysis temperature. The detail of the relative composition ratio of different types of nitrogen in the various catalysts was presented in Table 2. It can be seen that the relative

Table 2 Relative atomic ratios of N species of PI-based catalysts under different heat-treatment temperatures from XPS analysis.

N1s (at%)	Pyridinic nitrogen	Quaternar ynitrogen	C-N^+ nitrogen
PI-Fe-BP-700	64.3	29.7	6.0
PI-Fe-BP-800	52.2	32.5	15.3
PI-Fe-BP-900	33.6	54.1	12.3
PI-Fe-BP-1000	31.1	49.8	19.1

ratio of pyridinic N decreases to 33.6 at% from 64.3 at% and the ratio of quaternary N increases to 54.1 at% from 29.7 at% as the pyrolysis temperature raised from 700 to 900 ℃. That is because that the pyridinic N groups are not heat-resistant and may convert to quaternary N and C-N^+ at higher pyrolysis temperatures. Hence, the relative content of C-N^+ also had a trend of increase as the temperature increases. Based on the observation about the electrochemical ORR performance (the ORR activity of the catalysts prepared at different temperatures increased with increasing temperature to 900 ℃, and the PI-Fe-C-900 with highest ratio (54.1 at%) of quaternary N exhibits most excellent ORR performance among all the catalysts.), it is not hard to find that quaternary N plays the most important role in ORR activity and higher atomic ratio of quaternary N contributes to higher ORR activity.

The above results were in good agreement with observations from Chung et al. that the quaternary-type nitrogen were expected to lower the carbon band gap energy and may act as the ORR active site [38]. And some recent researches on nitrogen-doped carbon catalysts also proposed that the quaternary-type nitrogen promoted catalytic activity [39, 40]. The ORR active mechanism of quaternary N had been clearly illuminated by Deng et al. The relative electronegativity of quaternary N atoms reduces the electron density on the adjacent C nuclei, which helps electrons transfer from the adjacent C to N atoms, and N back donates electrons to adjacent C p_z orbitals [41]. The donation and back donation processes not only facilitate O_2 dissociation on the adjacent C atoms, but also help forming a strong chemical bond between O and C[41, 42].

In the present study, the PI-Fe-BP-900 catalyst was compared with that of a commercial Pt/C (10 wt%) catalyst in Fig. 7a. The ORR polarization curve shown that PI-Fe-BP-900 had a high onset potential of 0.92V and a half-wave potential of 0.78V, about 60 mV and 35 mV lower than that of Pt/C catalyst. The mass activity of the catalyst at 0.80 V is 2.13 A·g^{-1} and kinetic currents derived from the mass transport correction of the disk currents(Fig. 7b) show a Tafel slope of 66 mV per decade at low currents, close to the 70 mV per decade for the Pt/C catalyst. The comparable ORR onset-

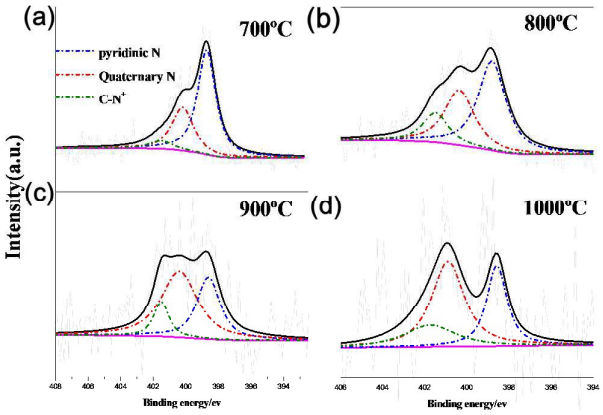

Fig.6 (a-d) The corresponding N 1s XPS spectra of these catalysts (a for PI-Fe-BP-700, b for PI-Fe-BP-800, c for PI-Fe-BP-900, d for PI-Fe-BP-1000).

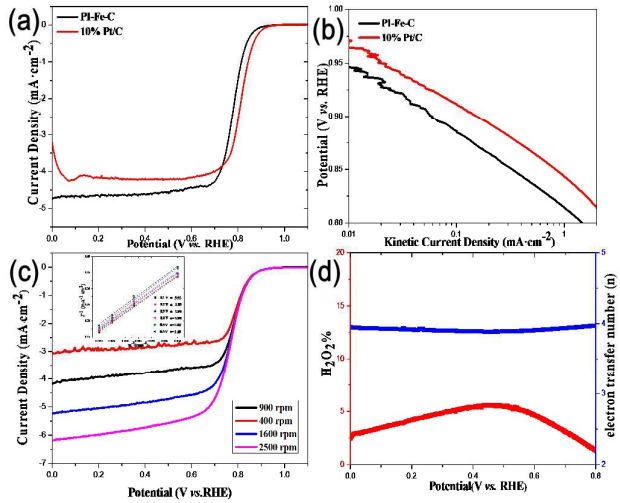

Fig.7 (a) ORR polarization curves for PI-Fe-BP-900, Pt/C catalysts recorded in an O_2-saturated 0.1 M $HClO_4$ aqueous solution at a sweep rate of 10 mV $s^{-1}$and a rotation rate of 900 rpm. (b) Kinetic current densities versus potential derived from the mass transport correction of the corresponding RRDE disk currents (c) RDE measurements for PI-Fe-BP-900 with a rotation rate from 400 to 2500 rpm in an O_2-saturated 0.1 M $HClO_4$ aqueous solution at a sweep rate of 10 mV·s^{-1}. Inset shows K-L plots for PI-Fe-BP-900 at different potentials. (d) Percentage of peroxide in ORR on PI-Fe-BP-900 and the corresponding electron transfer number at various potentials.

potential and current densities to Pt/C catalyst demonstrate the catalyst is such a promising substitute for precious catalyst towards ORR.

It is well known that the ORR can proceed by two main routes: (i) 2-electron reduction to produce H_2O_2; direct 4-electron reduction to produce H_2O. The contribution of two pathways can be revealed by calculating the electron transfer numbers and determining the H_2O_2 yield. To quantitatively investigate the mechanism of the ORR on PI-Fe-C catalyst, the ORR curves of PI-Fe-BP-900 which was ultimately found to be the most active catatlyst were evaluated by using the rotating-disk electrode (RDE) technique in 0.1 M $HClO_4$ aqueous solution at different electrode rotation rates from 400 to 2500 rpm. As shown in Fig. 7c, the typical current density and electrocatalytic response of the PI-Fe-BP-900 increases as the rotation speeds increase, which can be explained by shortened diffusion distance at high speeds. The Koutecky–Levich (K–L) plots (j^{-1} vs. $\omega^{-1/2}$) are obtained from polarization curves at different potentials (insert in Fig. 7c). The linearity of the K-L plots and near parallelism of the fitting lines indicates first-order reaction kinetics toward the concentration of dissolved oxygen and similar electron transfer numbers for ORR at different potentials. The numbers of electrons transferred (n) per oxygen molecule involved can be calculated from the K–L equation (1), (2):

$$\frac{1}{j}=\frac{1}{j_k}+\frac{1}{j_d}=\frac{1}{j_k}+\frac{1}{B\omega^{1/2}} \quad (1)$$

$$B=0.62nFC_O D_0^{2/3}\nu^{-1/6} \quad (2)$$

where j is the total current density at a given electrode potential; j_k is the kinetic current density; j_d is the diffusion limiting current density; B is the Levich constant; ω is the electrode rotation rate (rpm); n is the number of electrons involved in the reaction; F (96485 C·mol^{-2}) is the Faraday constant ; D_0 ($1.93\times10^{-5}$$cm^2\cdot s^{-1}$)and C_O (1.26×10^{-6}mol·cm^{-3}) are the diffusion coefficient of dissolved oxygen and the bulk concentration of dissolved oxygen, respectively; and ν (1.009×10^{-2} $cm^2\cdot s^{-1}$)is the kinetic viscosity of the electrolyte[43]. The average n value is 3.90, adequately suggesting that the catalyst favours a 4-electron dominated oxygen reduction process rather than H_2O_2 production dominated one, which may be more appropriate for fuel cell application.

To gain insight into the ORR catalytic pathways of the catalyst, the rotating ring-disk electrode (RRDE) technique is used to quantitatively the monitor the formation of peroxide species (H_2O_2) during the ORR process. The hydrogen peroxide yield (%H_2O_2) and the electron number (n) during the ORR can be determined by the equations (3), (4):

$$H_2O_2(\%)=200\times\frac{I_R/N}{(I_R/N)+I_D} \quad (3)$$

$$n=4\times\frac{I_D}{I_D+I_R/N} \quad (4)$$

Where I_D is the disk current, I_R is the ring current, and N = 0.37 is the RRDE collection efficiency. As shown in Fig. 7d, the produced H_2O_2 for the catalyst PI-Fe-BP-900 is below 6% and the corresponding electron transfer number is calculated to be 3.92 over the potential of 0 V to 0.8 V, which was well consistent with the result obtained from the K-L plots based on RDE measurements. This further suggests that the catalyst basically catalyzes an efficiently direct 4-electron transfer ORR procedure, exhibiting prominently catalytic activity in acid medium.

4. Conclusion

In summary, a novel FeN_x/C ORR catalyst was fabricated through a one-step synthetic procedure by using the PI as the nitrogen donator, ferric chloride as the iron precursor and porous carbon as the support. The experimental results demonstrate that ORR activity of catalysts and the performance of single cells strongly depend on the specific surface area and porosity of catalysts. The pyrolysis temperatures have great impact on the N-containing functional groups, which play an important role on the catalyst's performance. It is remarkable that the obtained PI-Fe-BP catalyst exhibits excellent performance (onset potential of 0.92V and the half-wave potential 0.78V) towards ORR activity in acid medium. And the specific power of PI-Fe-BP was as high as 310 W·g^{-1} for PI-Fe-BP without back pressure applied. Combining with its low-cost precursors, simple and highly producible preparation, triazine-framework based PI–Fe-C catalyst is a promising alternative electrocatalyst for ORR in fuel cells.

Acknowledgements

This work was financially supported by Natural Science Foundation of China (21176111, 21476104), National Basic Research Program of China (973 Program, 2013CB632404), and Priority Academic Program Development of Jiangsu Higher Education Institutions. Jianguo Liu also thanks to the support of Qing Lan Project and Natural Science Foundation for Distinguished Young Scholars (BK 20150009) of Jiangsu Province, China.

Notes and references

1. M. Lefèvre, E. Proietti, F. Jaouen and J.-P. Dodelet, *Science*, 2009, **324**, 71-74.
2. B. C. Steele and A. Heinzel, *Nature*, 2001, **414**, 345-352.
3. G. Wu, K. L. More, C. M. Johnston and P. Zelenay, *Science*, 2011, **332**, 443-447.
4. R. Bashyam and P. Zelenay, *Nature*, 2006, **443**, 63-66.
5. M. K. Debe, *Nature*, 2012, **486**, 43-51.
6. F. Jaouen, E. Proietti, M. Lefèvre, R. Chenitz, J.-P. Dodelet, G. Wu, H. T. Chung, C. M. Johnston and P. Zelenay, *Energy & Environmental Science*, 2011, **4**, 114-130.
7. A. Chen and P. Holt-Hindle, *Chem. Rev*, 2010, **110**, 3767-3804.
8. Y. X. Chen, A. Lavacchi, S. P. Chen, F. di Benedetto, M. Bevilacqua, C. Bianchini, P. Fornasiero, M. Innocenti, M. Marelli and W. Oberhauser, *Angewandte Chemie International Edition*, 2012, **51**, 8500-8504.
9. L. Feng, Y. Yan, Y. Chen and L. Wang, *Energy & Environmental Science*, 2011, **4**, 1892.
10. F. Jaouen, J. Herranz, M. Lefevre, J. P. Dodelet, U. I. Kramm, I. Herrmann, P. Bogdanoff, J. Maruyama, T. Nagaoka, A. Garsuch, J. R. Dahn, T. Olson, S. Pylypenko, P. Atanassov and E. A. Ustinov, *ACS applied materials & interfaces*, 2009, **1**, 1623-1639.
11. A. J. Bard and L. R. Faulkner, *Electrochemical methods: fundamentals and applications*, Wiley New York, 1980.
12. P. G. Bruce, S. A. Freunberger, L. J. Hardwick and J. M. Tarascon, *Nature materials*, 2012, **11**, 19-29.
13. J. Xiao, D. Mei, X. Li, W. Xu, D. Wang, G. L. Graff, W. D. Bennett, Z. Nie, L. V. Saraf, I. A. Aksay, J. Liu and J. G. Zhang, *Nano letters*, 2011, **11**, 5071-5078.
14. S. Blankenburg, M. Bieri, R. Fasel, K. Mullen, C. A. Pignedoli and D. Passerone, *Small*, 2010, **6**, 2266-2271.
15. N. Du, H. Zhang, B. D. Chen, X. Y. Ma, Z. H. Liu, J. B. Wu and D. R. Yang, *Advanced Materials*, 2007, **19**, 1641-1645.
16. J. Liu, Z. Guo, F. Meng, T. Luo, M. Li and J. Liu, *Nanotechnology*, 2009, **20**, 125501.
17. Y. J. Wang, D. P. Wilkinson and J. Zhang, *Chemical reviews*, 2011, **111**, 7625-7651.
18. C. Koenigsmann, A. C. Santulli, K. Gong, M. B. Vukmirovic, W. P. Zhou, E. Sutter, S. S. Wong and R. R. Adzic, *Journal of the American Chemical Society*, 2011, **133**, 9783-9795.
19. Y. Sun, Q. Wu and G. Shi, *Energy & Environmental Science*, 2011, **4**, 1113.
20. Z. S. Wu, S. Yang, Y. Sun, K. Parvez, X. Feng and K. Mullen, *Journal of the American Chemical Society*, 2012, **134**, 9082-9085.
21. S. Yang, L. Zhi, K. Tang, X. Feng, J. Maier and K. Müllen, *Advanced Functional Materials*, 2012, **22**, 3634-3640.
22. J. Zhang, K. Sasaki, E. Sutter and R. R. Adzic, *Science*, 2007, **315**, 220-222.
23. B. Lim, M. Jiang, P. H. Camargo, E. C. Cho, J. Tao, X. Lu, Y. Zhu and Y. Xia, *Science*, 2009, **324**, 1302-1305.
24. S. Chu, Y. Wang, Y. Guo, P. Zhou, H. Yu, L. Luo, F. Kong and Z. Zou, *J. Mater. Chem.*, 2012, **22**, 15519-15521.
25. J.-D. Xiao, L.-G. Qiu, Y.-P. Yuan, X. Jiang, A.-J. Xie and Y.-H. Shen, *Inorganic Chemistry Communications*, 2013, **29**, 128-130.
26. A. Trewin and A. I. Cooper, *CrystEngComm*, 2009, **11**, 1819-1822.
27. O. K. Farha, A. M. Spokoyny, B. G. Hauser, Y.-S. Bae, S. E. Brown, R. Q. Snurr, C. A. Mirkin and J. T. Hupp, *Chemistry of Materials*, 2009, **21**, 3033-3035.
28. H. Peng, Z. Mo, S. Liao, H. Liang, L. Yang, F. Luo, H. Song, Y. Zhong and B. Zhang, *Scientific Reports*, 2013, **3**.
29. G. Wu, K. L. More, C. M. Johnston and P. Zelenay, *Science*, 2011, **332**, 443-447.
30. Y. Hu, J. O. Jensen, W. Zhang, L. N. Cleemann, W. Xing, N. J. Bjerrum and Q. Li, *Angewandte Chemie International Edition*, 2014, **53**, 3675-3679.
31. Y. Tan, C. Xu, G. Chen, X. Fang, N. Zheng and Q. Xie, *Advanced Functional Materials*, 2012, **22**, 4584-4591.
32. N. Ranjbar Sahraie, J. P. Paraknowitsch, C. Gobel, A. Thomas and P. Strasser, *Journal of the American Chemical Society*, 2014, **136**, 14486-14497.
33. G. Faubert, R. Côté, J. Dodelet, M. Lefevre and P. Bertrand, *Electrochimica Acta*, 1999, **44**, 2589-2603.
34. X. Su, J. Liu, Y. Yao, Y. You, X. Zhang, C. Zhao, H. Wan, Y. Zhou and Z. Zou, *Chemical communications*, 2015, **51**, 16707-16709.
35. H. C. Huang, I. Shown, S. T. Chang, H. C. Hsu, H. Y. Du, M. C. Kuo, K. T. Wong, S. F. Wang, C. H. Wang and L. C. Chen, *Advanced Functional Materials*, 2012, **22**, 3500-3508.
36. F. Razmjooei, K. P. Singh, E. J. Bae and J.-S. Yu, *J. Mater. Chem. A*, 2015, **3**, 11031-11039.
37. V. Nallathambi, J.-W. Lee, S. P. Kumaraguru, G. Wu and B. N. Popov, *Journal of Power Sources*, 2008, **183**, 34-42.
38. H. T. Chung, C. M. Johnston, K. Artyushkova, M. Ferrandon, D. J. Myers and P. Zelenay,

Electrochemistry Communications, 2010, **12**, 1792-1795.
39. J.-i. Ozaki, T. Anahara, N. Kimura and A. Oya, *Carbon*, 2006, **44**, 3358-3361.
40. K. Lee, L. Zhang, H. Lui, R. Hui, Z. Shi and J. Zhang, *Electrochimica Acta*, 2009, **54**, 4704-4711.
41. D. Deng, L. Yu, X. Pan, S. Wang, X. Chen, P. Hu, L. Sun and X. Bao, *Chemical communications*, 2011, **47**, 10016-10018.
42. L. Lai, J. R. Potts, D. Zhan, L. Wang, C. K. Poh, C. Tang, H. Gong, Z. Shen, J. Lin and R. S. Ruoff, *Energy & Environmental Science*, 2012, **5**, 7936.
43. N. Marković, H. Gasteiger, B. Grgur and P. Ross, *Journal of Electroanalytical Chemistry*, 1999, **467**, 157-163.

Table of Content

A facile one-pot synthesis of ORR catalyst with high performance in fuel cell is proposed.